Molecular Dynamics Simulations of the Adipocyte Lipid Binding Protein Reveal a Novel Entry Site for the Ligand[†,‡]

Ran Friedman, Esther Nachliel, and Menachem Gutman*

Laser Laboratory for Fast Reactions in Biology, Department of Biochemistry, The George S. Wise Faculty of Life Sciences, Tel Aviv University, 69978 Ramat-Aviv, Tel Aviv, Israel

Received August 15, 2004; Revised Manuscript Received December 7, 2004

ABSTRACT: The adipocyte lipid binding protein (ALBP) binds fatty acids (FA) in a cavity that is inaccessible from the bulk. Therefore, the penetration of the FA necessitates conformational changes whose nature is still unknown. It was suggested that the lipid first enters through a "portal region" which consists of the αII helix and the adjacent tight turns. The initial event in the ligand binding must be the interaction of the lipid with the protein surface. To analyze this interaction, we have carried out three molecular dynamics simulations of the apo-ALBP, with a palmitate ion initially located at different positions near the protein surface. The simulation indicated that the ligand could adsorb to the protein in more than one location. Yet, in one case, the ligand managed to penetrate the protein by entering a newly formed cavity some 10 Å deep. The entry site is located near the N-terminus, at the junction between the loops connecting the β-strands. Further progression of the penetration seems to be arrested by the need for desolvation of the COOH end of the headgroup. Evolutionary analysis showed that amino acids in this entry site are well conserved. On the basis of these observations, we suggest that the ligand may enter the protein from a site other than the portal region. Furthermore, the rate-limiting step is proposed to be the desolvation of the FA polar headgroup.

The adipocyte lipid binding protein (ALBP)[1] comprises 1−3% of the soluble proteins in the adipose tissue. This protein binds small charged lipids and is involved in their storage, trafficking, and solubilization. The ALBP is built of 10 antiparrallel β-strands, which are connected via tight turns or α-helices, as seen in various structures of the apo and holo forms (*1*−*5*). The binding site for the fatty acids is located at a cavity which is buried inside the protein matrix, inaccessible from the bulk. In the bound state, the polar head is stabilized through hydrogen bonds with nearby amino acids (Arg126 and Tyr128) and the water molecules trapped inside the cavity (*6*, *7*), while the hydrophobic tail is bound in the cavity through hydrophobic contacts with the surrounding residues. Molecular dynamics (MD) simulations and continuum electrostatics calculations show that the anionic moiety of the bound lipid is protonated (*6*, *7*).

Kinetic measurements show that the substrate binding has to overcome an energy barrier of ∼7.0 kcal/mol (*8*). On the basis of the similarity between the structures of the holo and apo forms of the protein, it was suggested that this barrier is due to the conformational change needed to accommodate the lipid. The nature of this conformational change is yet unknown, but it was suggested that the lipid first enters through an entry site termed the portal region, consisting of the αII helix, and the tight turns composed of residues 55−58 and 74−78 (*2*, *5*, *9*).

The structure of the holoprotein, with the palmitic acid bound [PDB entry 1lie (*3*)], is shown in Figure 1. Examination of the location of the fatty acids indicates that the carboxylate head of the lipid is located near Arg126, Tyr128, and Cys117 (*10*), while the lipid tail is located among residues D77, V32, F57, and K59, which are part of the portal region. The suggestion that the ligand accesses the protein through the portal region was supported by structural evidence (*9*) and by mutagenesis studies (*5*).

It is reasonable to assume that the initial interaction between the protein surface and the lipid involves both electrostatic attraction (*11*) and hydrophobic interactions. Our previous studies of the dynamics of ions on the surface of globular protein S6 have shown that the protein surface features several ion attractor sites, and that ions are liable to move directly from site to site (*12*). Following these observations, we were motivated to study the dynamics of larger ionic ligands, such as fatty acids (FA), on the protein surface; previous simulations of the ALBP and of other FA binding proteins (FABPs) did not address the dynamical properties of the palmitate on the protein surface (*6*, *7*, *13*−*19*).

[†] This research is supported by the Israel Science Foundation (Grant 427/01-1) and the United States-Israel Bi-National Science Foundation (Grant 2002129). We acknowledge the use of computer resources belonging to the High Performance Computing Unit, a division of the Inter University Computing Center, which is a consortium formed by research universities in Israel, and to the Bioinformatics Unit of Tel Aviv University. R.F. acknowledges the Colton Foundation for its support through the Colton Scholarship.

[‡] Any of the final structures and intermediate structures that are given in the figures can be obtained in PDB format upon request.

* To whom correspondence should be addressed: Laser Laboratory for Fast Reactions in Biology, Department of Biochemistry, The George S. Wise Faculty of Life Sciences, Tel Aviv University, 69978 Ramat Aviv, Tel Aviv, Israel. Phone: +972-3-6409875. Fax: +972-3-6409875. E-mail: me@hemi.tau.ac.il.

[1] Abbreviations: ALBP, adipocyte lipid binding protein; FA, fatty acid; FABP, fatty acid binding protein; MD, molecular dynamics; SASA, solvent accessible surface area; HDS, hexadecanesulfonate.

10.1021/bi048236t CCC: $30.25
Published on Web 02/22/2005

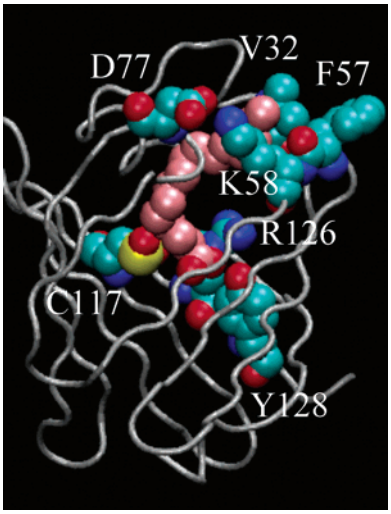

FIGURE 1: Structure of the adipocyte lipid binding protein with palmitic acid bound [PDB entry 1LIE (*3*)]. The FA is colored pink. The carboxyl group is located near the hydroxyl's oxygen of Tyr128. The lipid tail is located among residues Asp77, Val32, Phe57, and Lys58. Residues Arg126 and Cys117, which form part of the binding pocket, are also displayed.

For this reason, we have carried out three independent MD simulations of the apo-ALBP (for details, see Table 1). In one of the simulations, the lipid (palmitate) was initially positioned with its carboxylate near the portal region. In the other two, the FA was initially positioned at other locations, a few angstroms from a positively charged amino acid (Figure 2). One of these sites was chosen so that the lipid tail (but not the carboxylate head) will be located close to the portal region (simulation MD_A). The other site was arbitrarily located on the opposite side of the protein (simulation MD_I). It was found that in one case (simulation MD_I) the FA could penetrate the protein surface, but failed to arrive at the crystallographic binding site. Assuming that the inability of the ligand to further penetrate the protein might be due to the high energy cost involving the desolvation of the charged carboxyl head of the FA, the simulation was rerun with a protonated ligand. However, no further penetration was observed, thus suggesting that the solvation of the neutral headgroup still retards the process. This suggestion was tested by eliminating the partial charges of the atoms of the FA's carboxylate. In this case, further penetration of the ligand was observed.

In the two other simulations (MD_P and MD_A), the lipid did not penetrate the protein outer shell, but rather adsorbed to the protein surface, forming a complex that was stable as long as the simulations continued (i.e., 6−8 ns). The results suggest that the FA can enter the protein from a site other than the suggested portal region. Furthermore, the rate-limiting step, for the initial penetration of the ligand, is proposed to be the desolvation of the lipid's polar headgroup.

MATERIALS AND METHODS

Molecular Dynamics Simulations. The molecular dynamics (MD) simulations were performed using the GROMACS package of programs: either GROMACS 3.1.4 or GROMACS 3.2.1 (*20*−*22*), with the GROMACS force field, which is a modified version of the GROMOS87 force field (*23*−*27*). The calculations were carried out using the structure of the apo-ALBP (PDB entry 1LIB) determined by Xu and co-workers (*2*) that was downloaded from the Protein Data Bank (*28*). The lipid topology files, as needed in Gromacs, were prepared using the PRODRG server (*29*). The protein and the ligand were embedded in a box containing the SPC water model (*30*) that extended to at least 8 Å (in runs MD_A and MD_I) or 10 Å (in run MD_P) between the solutes and the edge of the box. The total number of water molecules was between 6898 and 9986. Ten Na^+ and 11 Cl^- ions were added to the system by replacing water molecules in random positions, thus making the whole system neutral.

Prior to the dynamics simulation, internal constraints were relaxed by energy minimization. Following the minimization, an MD equilibration run was performed under position restraints for 20 ps. An unrestrained MD run was then initiated. The first 100 ps of the run was treated as a further equilibration simulation, and the remainder were saved and used for the analysis. During the MD runs, the LINCS algorithm (*31*) was used to constrain the lengths of hydrogen-containing bonds; the waters were restrained using the SETTLE algorithm (*32*). The time step for the simulations was 2 fs. The simulations were run under NPT conditions, using Berendsen's coupling algorithm (*33*) for keeping the temperature and pressure constant ($P = 1$ bar, $\tau_P = 0.5$ ps; $T = 300$ K, $\tau_T = 0.1$ ps). VDW forces were treated using a 12 Å cutoff. Long-range electrostatic forces were treated using the particle mesh Ewald method (*34*). The coordinates were saved every 0.5 ps.

Two of the simulations (MD_H1 and MD_H2) were started from configurations extracted from simulation MD_I after 4 and 9 ns of the simulation, respectively. In these simulations, the lipid was protonated by adding a single proton to one of the carboxylate oxygens using InsightII (Accelrys, Inc., San Diego, CA). Following the protonation, a single Na^+ ion, selected randomly, was deleted from the system to ensure that its overall charge remains neutral. The systems were then energy minimized and equilibrated as described above, prior to production MD runs being carried out.

Simulation MD_N was started from the configuration extracted from simulation MD_I after 5 ns of the simulation. In this simulation, the partial charges of the carboxylate group were eliminated. The simulation setup was performed by using the same procedures as in simulations MD_H1 and MD_H2.

The analysis of the simulations was performed using the analysis tools provided in the Gromacs package. Where the electrostatic contributions to interaction energies are considered, we refer to only the short-range interactions (up to 10 Å). Long-range interactions between individual molecules cannot be extracted from the simulations due to the usage of particle mesh Ewald [PME (*34*)] treatment for the calculation of long-range electrostatics. It should be mentioned that over the whole run, the long-range interactions contributed, on the average, less than 12% of the total electrostatic energies.

Analysis of the Evolutionary Conservation of the ALBP. The normalized conservation scores of the amino acid residues of the ALBP were calculated using the ConSurf server (*35*). Amino acid conservation scores were calculated by the maximum likelihood method. A single iteration of PSI-blast was run. The PSI-blast cutoff was set to 1E-10, yielding a total of 71 homologous sequences that were used

Table 1: Summary of the MD Simulations

simulation	ligand starting point	duration (ns)	ligand protonation state
MD_P	near the portal region, with the carboxylate head located 6.2 Å from the nearest HZ atom of Lys58, which is part of the portal region	10	unprotonated
MD_A	arbitrary position near the protein surface, 4.9 Å from HZ of Lys9	6	unprotonated
MD_I	arbitrary position near the protein surface, 7.8 Å from HZ of Lys65	11	unprotonated
MD_H1	a continuation of the simulation marked as MD_I, starting from $t = 4$ ns	5	protonated
MD_H2	a continuation of the simulation marked as MD_I, starting from $t = 9$ ns	3	protonated
MD_N	a continuation of the simulation marked as MD_I, starting from $t = 5$ ns, in which the palmitate is modeled without any charges on the terminal oxygens	8	unprotonated, but not charged

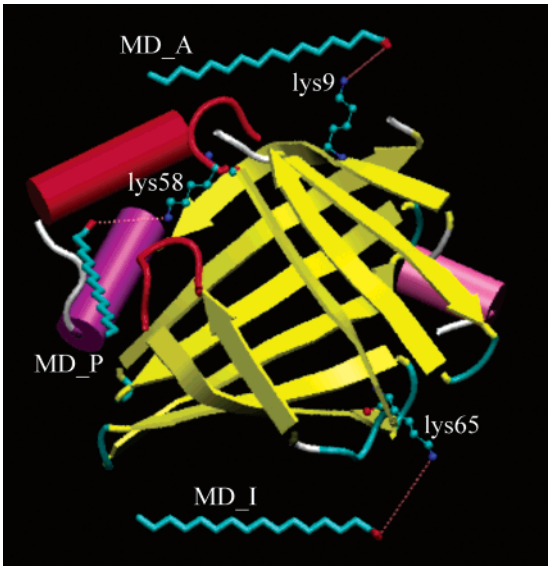

FIGURE 2: Starting conditions of the MD simulations. The protein is shown with the palmitic acid in three different positions, corresponding to three different simulations (MD_P, MD_A, and MD_I; see Table 1). The portal region is colored red. The positive residues, which are located in the closest positions to the palmitate carboxylates, are displayed in a ball-and-stick representation.

in the analysis. The list of those sequences and the conservation scores of all the amino acids of the ALBP are provided in the Supporting Information.

Graphical Presentations. All protein figures were created using VMD (*36*).

RESULTS

Molecular Dynamics Runs of the ALBP with Unprotonated Palmitate. At physiological pH, the fatty acids are ionized. Thus, the initial simulations were carried out with the palmitate state of the ligand. Three MD runs were performed, differing in the initial location of the ligand. In the first run, the palmitate was located near the portal region (*9*), while the other two were initiated with the ligand placed on other locations a few angstroms from a positively charged amino acid (Figure 2). In all cases, the initial location of the FA was not in contact with the protein and the distance from the protein was followed with time.

At the beginning of run MD_P, the ligand executed a random walk, but after 2 ns, the ligand approached the protein and the minimal distance between them was reduced to 0.3−0.4 nm. The very same features were also noticed in simulation MD_A. After a very short period, the ligand was attracted to the vicinity of the protein, and except for a brief

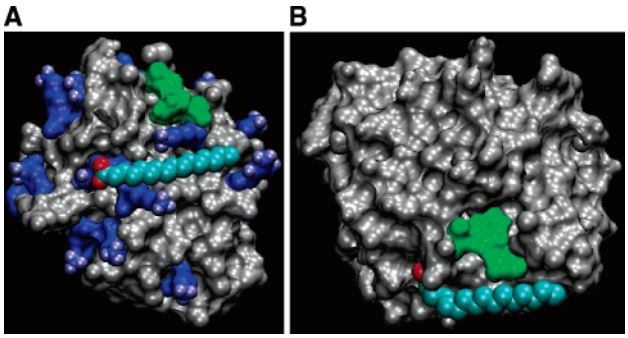

FIGURE 3: (A) Structure of the adipocyte lipid binding protein, with palmitate, after 9 ns of simulation (simulation MD_P, starting with the palmitate near the portal region). Residues Val32 and Phe57, close to which the lipid appeared to have entered its binding site in the X-ray structure of the holoenzyme (see Figure 1), are colored green. Lysine and arginine residues are colored blue, with their terminal hydrogens highlighted. The lipid is docked to the protein surface by hydrophobic interactions and by a formation of a salt bridge with Arg78. (B) Structure of the adipocyte lipid binding protein, with palmitate, after 6 ns of simulation (simulation MD_A). The palmitate does not penetrate the protein envelope.

period between 2100 and 2700 ps, the minimal distance between the ligand and the protein was comparable to the van der Waals contact distance. In both simulations, after some wiggling of the ligand's tail, the hydrophobic section was practically fixed to the surface while the headgroup retained a higher degree of freedom.

The adsorption sites, corresponding with MD_P and MD_A, are shown in Figure 3. In both cases, the lipid tail is adsorbed to the protein surface through hydrophobic interactions with the nearby atoms, while the carboxyl head interacts either with positive residues or with the solvent. Apparently, apart from the binding configurations determined in the crystal structure of the holoprotein (*2*−*4*), charged FAs can bind to the protein in other, nonspecific locations.

To find the forces which stabilize the adsorption, the contributions of the electrostatic attraction and the van der Waals interactions were calculated during the simulations, and the results are presented in Figure 4. The interaction of the ligand with the protein in simulation MD_P (panel A) represents brief bursts of electrostatic attractions and persistent van der Waals stabilization. It is of interest to note that the stabilization is not achieved in one step, as if the ligand is searching the local environment for the most stable location. The same features are also noticed in the other simulation. The interaction of the ligand with the protein in simulation MD_A (Figure 4B) took place during the equilibration phase of the simulation, and retained the same position for the rest of the simulation. While it hardly moves

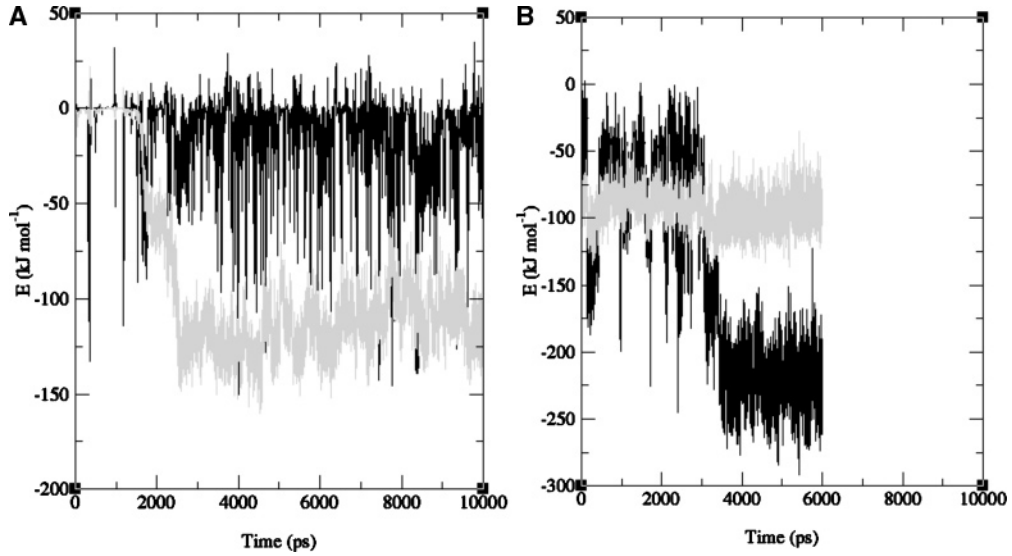

FIGURE 4: Electrostatic (black) and VdW (gray) contributions to the energies of interaction between the protein and the palmitate in simulations MD_P (A) and MD_A (B).

with respect to the surface, it is clear that the system is optimized by both electrostatic and van der Waals interactions. The configuration that dominates through the end of the simulation had evolved after ~2.5 ns of searching for the proper position. In contrast to the previous simulation, the stability involves a favorable electrostatic term. Considering that the ligand is an ampiphyll, the two sites represent its dual nature. In one case, the stabilization is strongly hydrophobic, while in the other case, we notice also the electrostatic contribution to the stability.

The third simulation, MD_I, evolved differently. During the first 2 ns, the FA was adsorbed to the protein surface. However, following the adsorption, the protein responded by altering its structure, opening a cavity through which the hydrophobic tail of the ligand started to penetrate into the protein (Figure 5). The point of insertion was close to the N-terminus (Figure 5E), a site where the loops connecting the β-strands meet and form a loose spot, where minor motions of the strands can create an opening. Figure 5A−D presents a series of snapshots taken during 200 ps of the simulation time. Panel A depicts the first state, where the ligand is adsorbed to the protein by its full length; 50 ps later (panel B), a pore has already been formed near the tail of the FA, and with progression of time, the ligand is rapidly inserted into the protein surface, tail first. This phase is almost finished with 200 ps. From that time point forward, the process of penetration hardly evolved. Up to 7 ns of simulation time, the ligand remained with the carboxylate protruding into the bulk (see panel E). At ~7 ns, the ligand folded on itself and assumed a bent configuration (panel F). This state was maintained until the simulation was terminated at 11 ns. We assumed that once the first penetration took place, the protein had made its adjustment to the presence of the ligand, and the various states that were noticed during the rest of the simulation were structure fluctuations of the protein−ligand system, which randomly searched the equipotential configuration space.

The electrostatic and hydrophobic contributions to the energy of interaction between the protein and the ligand were followed throughout the simulation, and the results are presented in Figure 6. During the first 2 ns, when the ligand is coming into contact with the protein, we observed brief bursts of electrostatic interactions, which were concomitant with a steady stabilization of the system by van der Waals interactions. For the rest of the simulation time, the system is fairly stable, except for some further stabilization at ~6−7 ns due to van der Waals interactions. In this final phase, the headgroup assumed a location where it can better interact with polar residues on the surface, as detected by sporadic changes in the electrostatic interaction energies.

Variation in the Hydrophobic Solvent Accessible Surface. The adsorption of the lipid to the protein surface, which occurred in all three simulations, is entropically unfavorable as it limits the mobility of the ligand. Hence, an enthalpic advantage must be involved in the process. The energies for the interaction between the protein and the ligand are favorable (Figure 4), yet these functions had not accounted for another major factor, the interactions with the solvent which are quantitated by the reduction of the hydrophobic solvent accessible surface area (SASA). The variation of SASA throughout the three simulations is presented in Figure 7.

The adsorption of the ligand in simulation MD_P, presented in panel A, exhibits the same features noticed in Figure 4. The hydrophobic sections of the ligand−protein system come into contact and reduce the surface where water is in direct contact with the hydrophobic surface. The energy gain of the process is as high as ~10 kcal/mol (calculated using the g_sas program in Gromacs). In the case of simulation MD_I, the reduction of the SASA makes a smaller contribution. In the case of simulation MD_A, the ligand had already been adsorbed to the protein surface during the equilibration phase, and no further reduction in the SASA is evident.

Molecular Dynamics Runs of the ALBP with Protonated Palmitate. During simulation MD_I, the ligand penetrated the protein. However, in its final location, it was still quite distant from the crystallographically determined binding site (see Figure 5G,H). One of the reasons that the ligand penetration was arrested is the strong interaction of the carboxylate moiety with the water. What is more, several studies have indicated that the palmitic acid is protonated in the holoprotein (*6*, *7*). Hence, to evaluate whether the

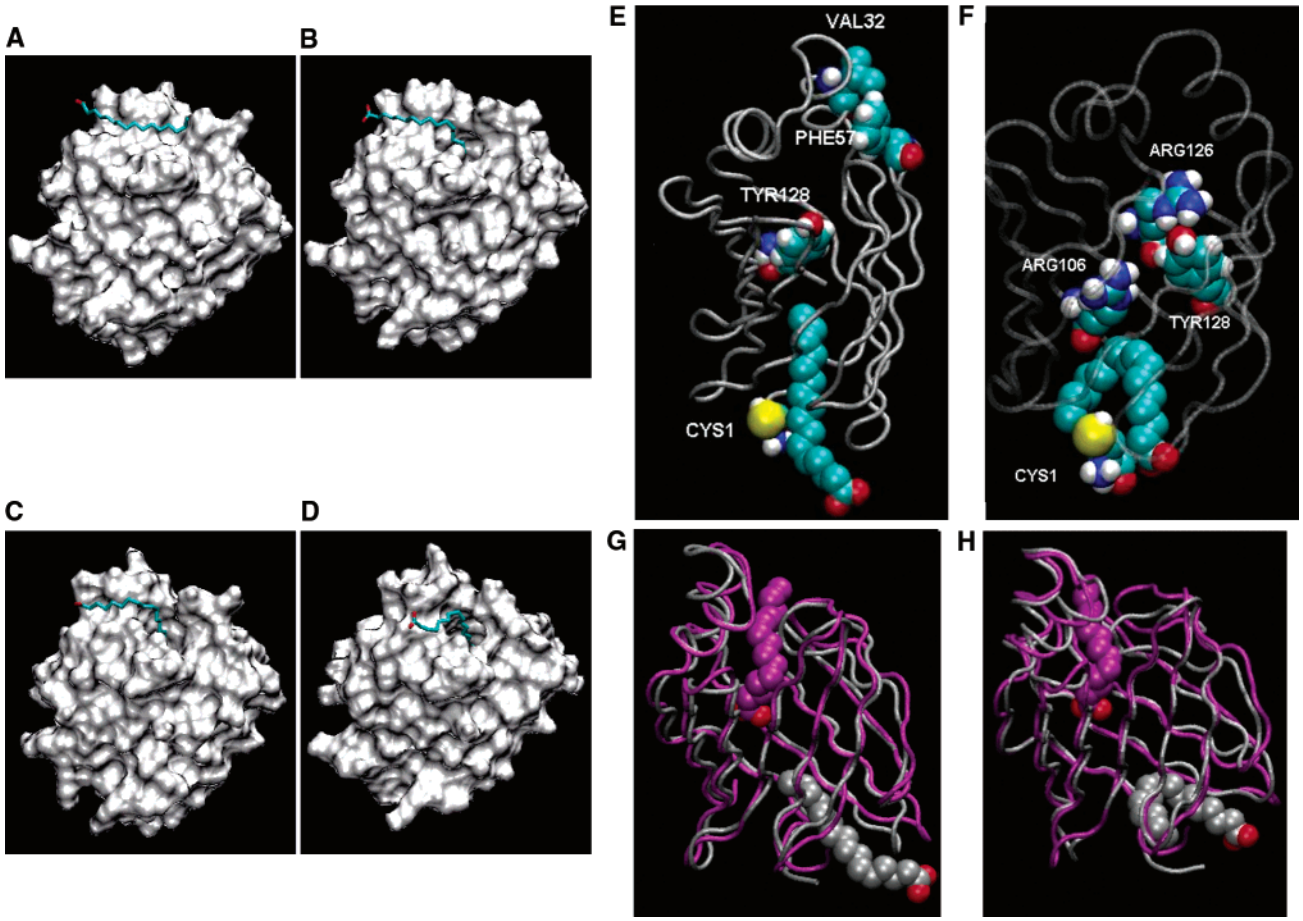

FIGURE 5: (A−D) Insertion of the lipid into the protein, presented as a temporal series at 2, 2.05, 2.1, and 2.2 ns. A movie displaying the penetration of the ligand between 2 and 4 ns is given in the Supporting Information. (E) Structure of the adipocyte lipid binding protein, with palmitate, after 5 ns of simulation (simulation MD_I). The hydrophobic tail of the lipid has already penetrated into the protein, near Cys1. (F) Structure of the adipocyte lipid binding protein, with palmitate, after 10 ns of simulation (simulation MD_I). The lipid is folded into a pocket inside the protein. The carboxylate is stabilized through a salt bridge formed with the amine group of Cys1. (G and H) Structure of the adipocyte lipid binding protein, with palmitate, after 5 and 11 ns of simulation (gray) aligned over the structure of the holoprotein (purple). The ligand stays in the U-shaped folded state during the final 4 ns of the simulation, and no exit or entry is observed.

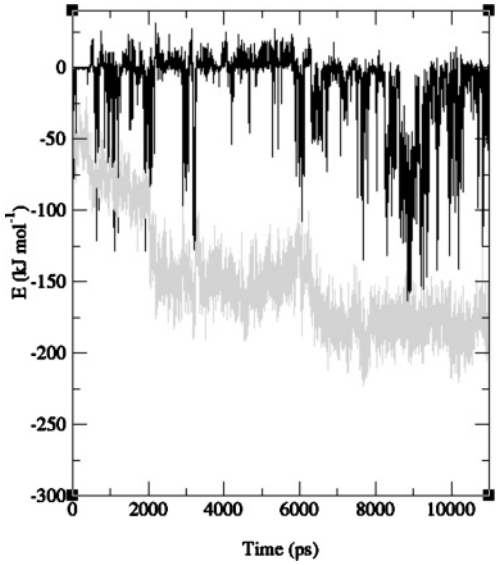

FIGURE 6: Electrostatic (black) and VdW (gray) contributions to the energies of interaction between the protein and the palmitate in simulation MD_I.

inability of the palmitate to further penetrate the protein surface was due to its charge, a proton was added to an intermediate structure obtained from the MD_I simulation.

Two different runs were performed on this system: MD_H1 and MD_H2. The first one was initiated after the lipid had buried itself in a narrow cavity (see Figure 5E,G), while in the second one, a proton was added to the carboxylate after the ligand had folded inside a pocket as in Figure 5F. Both simulations were continued with the protonated carboxylates, but as seen in Figure 8, no further penetration was observed and the headgroup remained well within the aqueous phase. Apparently, the neutralization of the carboxylate is not sufficient to overcome the energy barrier needed for the insertion of the headgroup into the low-dielectric protein matrix. Both the protonated and unprotonated FA were stabilized by interactions with the water. What is more, both the carboxylate and the carboxylic state of the ligand form salt bridges with adjacent positive residues or hydrogen bonds with nearby polar residues (see Figures 5F and 8B). Thus, an examination of the headgroup-water interactions suggests that the rate-limiting step of the ligand insertion will be the desolvation of the COOH head of the ligand.

Molecular Dynamics Runs of the ALBP with a Nonpolar Headgroup. To test the assumption that the inability of the FA to fully penetrate the protein surface was due to the hydrophilic nature of its headgroup, another MD run was conducted, starting from the intermediate structure seen in

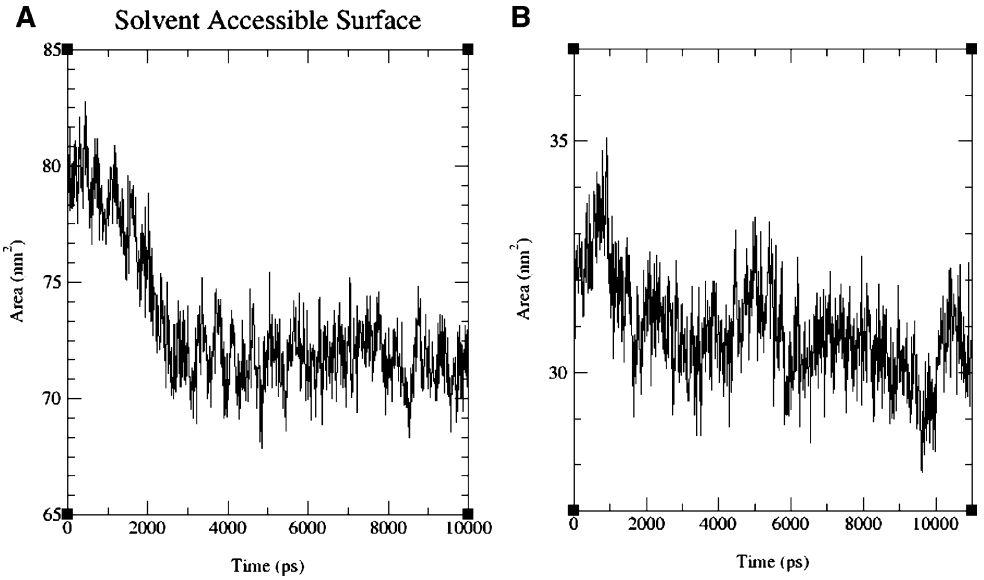

FIGURE 7: Total hydrophobic SASA of the protein and the palmitate (together) as a function of simulation time (A) during the MD run labeled MD_Portal and (B) during the MD run labeled MD_I.

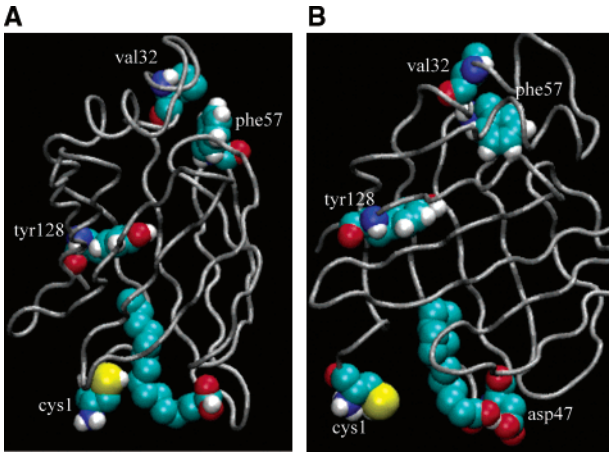

FIGURE 8: (A) Structure of the adipocyte lipid binding protein, after 5 ns of simulation with protonated palmitic acid (simulation MD_HI; see Table 1). Despite the protonation, only the hydrophobic tail of the ligand is located inside the protein. (B) Structure of the adipocyte lipid binding protein, with protonated palmitic acid, after 3 ns of simulation (simulation MD_H2; see Table 1). Note that the FA is located in a pocket on the protein surface and its polar head is hydrogen bonded to Asp47 (compare to Figure 5F, where the unprotonated headgroup interacts with Cys1).

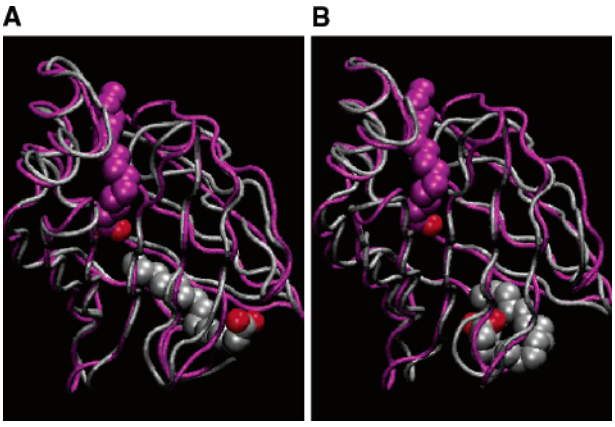

FIGURE 9: Structure of the adipocyte lipid binding protein, with palmitate, after 5 (A) and 8 ns (B) of simulation MD_N (gray) aligned over the structure of the holoprotein (purple). The ligand fully penetrates the protein surface, and then starts folding inside. Note that this is not a realistic simulation as the carboxylate oxygens bear no charges.

Figure 5E. In this simulation, the partial charges of the carboxylate group atoms were set to zero, and the system was allowed to evolve for 8 ns. During the run, the FA further penetrated the protein (see Figure 9A). After ~5 ns, the lipid started folding and the headgroup finally became internalized (Figure 9B). This simulation thus shows that the polar headgroup delays the acid in the solvent environment. However, it must be stressed that the latter simulation is basically nonrealistic as it eliminates a possible contribution of the polar atoms with Arg122 and Tyr128 that stabilize the ligand in the holoprotein structure.

DISCUSSION

Binding of the Fatty Acid to the Protein. Unlike many enzymes whose binding sites are fully accessible to the ligands in the bulk, the ALBP binding site is located in an inaccessible cavity, and the protein must execute some structural deformations so that the substrate will be able to enter. The initial step of the reaction is the adsorption of the ligand to the protein. This reaction was noticed in the three simulations. In two of them, the ligand remained in the adsorbed state on the surface. However, the adsorbed state does not seem to ensure penetration into the binding cavity. It seems that the protein conformational changes leading to the internalization of the substrate are much more specific. Quite surprisingly, the event was noticed at an unsuspected location, in the junction of the β-strands antipodal to the portal region and very close to the short α-helix next to the N-terminus of the protein. When the FA was bound to this region, but not near the portal domain, there was a fast insertion of the lipid some 10 Å deep into the protein. The penetration of the hydrophobic section of the FA was not coupled with further reduction of the SASA.

The reaction between the FA and the protein had progressed only to partial internalization, which could not be further pushed, even by protonation of the carboxylate. Further penetration of the ligand was observed only when the partial charges of the headgroup were removed. This

artificial manipulation supports the conclusion that the hydration of the headgroup acts as a float that keeps the FA from penetrating deeply into the protein matrix.

For the ligand to fully penetrate the protein surface, the reaction had to overcome an energy barrier that we associate with desolvation of the carboxylate, most probably after the protonation of the headgroup. Indeed, there is a similarity between the solvation energy of palmitic acid [6.70 kcal/mol (*37*)] and the activation energy barrier associated with the binding of palmitate to ALBP [~7.0 kcal/mol (*8*)]. It should be noted that the desolvation energy of the acetate ion [CH_3COO^-, 82.48 kcal/mol (*38*)] is much higher. Apparently, the entry consists of protonation of the headgroup followed by the rate-limiting step of the ligand's headgroup desolvation before the process can be completed.

It is interesting to note that ALBP can bind negative ligands, such as hexadecanosulfonate (HDS). Crystal studies of HDS-bound ALBP show that the HDS occupy virtually the same site as palmitic acid (*3*). The binding of such a negative species seems improbable unless it is somehow neutralized. Woolf has previously suggested that in its bound state, the HDS is neutralized either through R126 or through a bridging hydronium (*7*). In the latter case, the hydronium species may accompany the HDS during its penetration into the protein, thereby lowering the activation energy.

Ligand Entry Site. Despite a wide range of ligand binding studies carried out with the ALBP (*5*, *11*, *39*−*42*), the location of the ligand entry site is still unknown. The portal region was suggested (*2*, *5*, *9*) to be the site where the ligand enters. This has not occurred in the reported MD simulations. However, we cannot exclude the possibility that the protein conformational motions, which allow the exposure of the ligand-binding cavity, are too slow to be observed during the time scale of ordinary MD simulations (*19*, *43*, *44*). On the other hand, we had observed a partial entry of the ligand at a very specific site within the time frame of the dynamics, and the reaction advanced up to a point where the experimental activation energy is compatible with the expected rate-limiting step which is the desolvation of the polar headgroup of the ligand. Accordingly, the site detected in this study should be considered as the site of entry.

The amino acids which are located less than 4 Å from the FA during its entry (i.e., between 2 and 3 ns of simulation time) are given in Table 2. Five residues (C1, F4, I42, L66, and L91) contact the FA in all the extracted structures between 2.2 and 3 ns. If the insertion of the ligand into the protein site through this entry site is a general mechanism, which also occurs in other fatty acid binding proteins, one should expect these residues to be evolutionarily conserved. To account for the evolutionary conservation of the entry region, as seen in the MD_I simulation, we analyzed the evolutionary conservation of the protein residues using the ConSurf server (*35*), using ALBP and other FABPs from different species. The server assigns a normalized conservation score from 1 (least conserved) to 9 (most conserved) to each of the protein's amino acids. The conservation scores of Cys1, Phe4, Ile42, Leu66, and Leu91, as well as the possible variants of these residues in the homologous proteins, are given in Table 3 (see also the Supporting Information). It can be seen that Cys1 and Phe4 are highly conserved, with no variants at those sites. However, it should be noted that gaps in the alignments are not taken into account in the calculation of the conservation scores. In the case of Cys1, it is conserved among proteins of the ALBP family from different organisms but is not found in other FABPs (and when the residue is absent, there was no replacement), while Phe4 is prevalent among different FABPs and conserved throughout all. Ile42, Leu66, and Leu91 are less conserved, but their variants are all bulky, hydrophobic residues that can stabilize the ligand through hydrophobic contacts. Ile42 and Leu91 are almost completely buried in the protein (i.e., their exposed surface area is very small); hence, their variants are expected to be hydrophobic even when ligand binding is not considered. On the other hand, Cys1, Phe4, and Leu66 are surface residues, and it is plausible to assume that their high conversion scores (see Table 3) are due to their role in ligand binding.

Cys1 and Phe4 were previously subjected to chemical modifications and mutations. Buelt and Bernlohr have found that modification of Cys1 by *N*-ethylmaleimide (NEM) did not decrease the apparent affinity of the protein for oleic acid (*10*). Furthermore, Veerkamp and colleagues studied the relative binding of the FA to the protein and the oxidation rates of the FA in the mitochondria, in the presence of wild-type and mutant heart lipid binding proteins (*45*, *46*). Only minor differences were observed between the wild-type protein and the F4S and F4E mutants. It must be stated that both findings are not in contrast to the suggested site of entry.

Table 2: Residues which Are <4 Å from the Ligand for Snapshot Structures Extracted at 200 ps Intervals, during the Main Part of the Ligand Penetration, between 2 and 3 ns from Simulation MD_I[a]

residue	$t = 2.0$ ns	$t = 2.2$ ns	$t = 2.4$ ns	$t = 2.6$ ns	$t = 2.8$ ns	$t = 3.0$ ns
C1	+	+	+	+	+	+
F4	−	+	+	+	+	+
M40	−	−	−	−	−	+
I42	−	+	+	+	+	+
V44	−	+	−	−	−	−
G46	−	−	+	+	+	+
D47	+	+	+	+	−	−
V49	−	+	−	−	+	−
I51	−	+	+	+	−	+
K65	+	−	−	−	−	+
L66	+	+	+	+	+	+
V68	+	−	−	−	−	−
L86	−	+	−	−	+	+
L91	−	+	+	+	+	+
R106	−	+	−	−	+	−
L113	−	−	−	−	+	−

[a] If a certain residue was located less than 4 Å from the nearest ligand atom, the relevant box bears a + sign; otherwise, it bears a − sign.

Table 3: ConSurf Conservation Scores and Possible Variants for the Five Residues which Are <4 Å from the Peptide during Its Entry into the Protein[a]

residue	conservation score	variants
Cys1	9	none[b]
Phe4	9	none
Ile42	8	F, L, M, V
Leu66	7	F, I, S, V, W
Leu91	5	F, I, M, V

[a] The ConSurf server assigns a normalized conservation score between 1 and 9 for each amino acid in the protein. The conservation scores of all the amino acids of the ALBP are given in the Supporting Information. [b] Cys1 is conserved among the ALBPs from different organisms, and is not found in other FABPs.

Table 4: Average Root-Mean-Square Deviations (rmsds) Calculated for All Heavy Atoms, Relative to the Crystal Structure of the Protein

simulation	rmsd (nm)		
	all	portal[a]	entry[b]
MD_I	0.198	0.220	0.251
MD_P	0.188	0.185	0.196
MD_A	0.178	0.180	0.190

[a] Residues 27−35, 55−58, and 74−78. [b] Residues 1, 4, 42, 66, and 91.

The mutations or modifications of residues in the alternative ligand entry site (Cys1 and Phe4) are not expected to change the binding equilibrium, since the ligand is not bound in that region. Dynamical changes in the initial process of ligand binding could not be observed in those studies, as the measured dynamics are orders of magnitude slower than the rate of entry of the lipid as deduced from the current study. According to the reported simulations, the initial entry takes only a few nanoseconds. The next phase predicted by the dynamics had an activation energy barrier of ∼7 kcal/mol or ∼12 k_BT. Such an energy barrier will lower the probability of the reaction to $\sim 8 \times 10^{-6}$. When that factor is combined with a nanosecond initial entry, the two-step event can still be over within 100 μs. Thus, the slow dynamics, measured on the minute time scale (*45*, *46*), will hardly be sensitive to a 100−1000-fold delay in the rate of entry.

Dynamics of the Protein during Ligand Adsorption and Insertion. The average root-mean-square deviations (rmsds) for the whole protein, the portal region, and these residues that contact the lipid at the entry site are given in Table 4. The rmsd of the residues at the entry site appears to be the highest in all three simulations of the protein. On the other hand, the rmsd of the portal region is hardly larger than the average for all residues, except for one simulation (MD_I). This indicates that the entry region was more mobile than the portal region in the current simulations.

Considering the results of the three different simulations, it seems that the FA can adsorb freely on more than one locus on the protein surface, and when a flexible site is selected, the hydrophobic interactions are sufficient to initiate a partial penetration. Yet, to form the final complex, such as the one found for the holoenzyme, the headgroup must be desolvated; this is the rate-limiting step of the initial binding event, and maybe even that of the overall process.

Ligand Entry Site in Different FABPs. There is a plethora of structural evidence suggesting that the portal region is involved in the insertion of the lipid in FABPs that come from different (i.e., non-adipose) tissues. Examples include mutation studies involving portal residues carried out with the heart FABP (*45*, *46*) and structural determinations of the intestinal FABP [I-FABP (*47*−*49*)]. In particular, residues in the portal region exhibited high mobility in the solution structures of the I-FABP (*47*), but not in the crystal structure of the protein (*50*). MD simulations of the I-FABP tend to agree better with the X-ray structure (*19*). As direct ligand exchange reactions were (and still are) impossible to simulate, the authors have analyzed water exchange between the protein and the bulk, taking advantage of the high mobility of the water compared to the palmitate. Three exchange sites were found; two of these sites were located near the portal region, and one was located on the opposite side, near the N-terminus. This site, termed the backbone portal by the authors, is located in the vicinity of the alternative entry site as suggested by our simulations, but not in the same place.

It was previously stated that "although a variety of studies are consistent with the notion that the FA enters and exits the binding cavity through the portal region, current evidence cannot exclude alternative pathways" (*51*). This statement is clearly supported by the simulations reported here.

CONCLUSIONS

Simulations of the interactions of the apo-ALBP with a palmitate ion on its surface revealed penetration of the protein surface by the ligand, at a site distant from the previously suggested portal region. The entry site is hydrophobic in nature, and the FA maintains contact with several hydrophobic residues as it penetrates the protein. These residues are evolutionarily conserved, and their variants are all of the same chemical nature.

When the lipid started to penetrate the protein surface, it could not reach the binding site within the nanosecond time frame, even if the lipid charge was eliminated. It is suggested that the rate-limiting step in the insertion of the FA into the protein is the desolvation of the FA carboxyl terminus. This suggestion is corroborated by the similarity between the desolvation energy of acetic acid [CH_3COOH, 6.7 kcal/mol (*38*)] and the enthalpy term in the activation energy barrier for the binding of palmitic acid to the ALBP (∼7 kcal/mol).

SUPPORTING INFORMATION AVAILABLE

A movie detailing the insertion of the palmitate into the ALBP protein, a list of the sequences which were used in the analysis of the evolutionary conservation of the ALBP amino acids, and a table which details the conservation scores for each amino acid, extracted from ConSurf. This material is available free of charge via the Internet at http://pubs.acs.org.

REFERENCES

1. Xu, Z., Bernlohr, D. A., and Banaszak, L. J. (1992) Crystal structure of recombinant murine adipocyte lipid-binding protein, *Biochem. J. 31*, 3484−3492.
2. Xu, Z., Bernlohr, D. A., and Banaszak, L. J. (1993) The adipocyte lipid-binding protein at 1.6-Å resolution. Crystal structures of the apoprotein and with bound saturated and unsaturated fatty acids, *J. Biol. Chem. 268*, 7874−7884.
3. LaLonde, J. M., Bernlohr, D. A., and Banaszak, L. J. (1994) X-ray crystallographic structures of adipocyte lipid-binding protein complexed with palmitate and hexadecanesulfonic acid. Properties of cavity binding sites, *Biochemistry 33*, 4885−4895.
4. LaLonde, J. M., Levenson, M. A., Roe, J. J., Bernlohr, D. A., and Banaszak, L. J. (1994) Adipocyte lipid-binding protein complexed with arachidonic acid. Titration calorimetry and X-ray crystallographic studies, *J. Biol. Chem. 269*, 25339−25347.
5. Ory, J., Kane, C. D., Simpson, M. A., Banaszak, L. J., and Bernlohr, D. A. (1997) Biochemical and crystallographic analyses of a portal mutant of the adipocyte lipid-binding protein, *J. Biol. Chem. 272*, 9793−9801.
6. Rich, M. R., and Evans, J. S. (1996) Molecular dynamics simulations of adipocyte lipid binding protein: Effect of electrostatics and acyl chain saturation, *Biochemistry 35*, 1506−1515.
7. Woolf, T. B. (1998) Simulations of fatty acid-binding proteins suggest sites important for function. I. Stearic acid, *Biophys. J. 74*, 681−693.
8. Richieri, G. V., Ogata, R. T., and Kleinfeld, A. M. (1996) Kinetics of fatty acid interactions with fatty acid binding proteins from adipocyte, heart, and intestine, *J. Biol. Chem. 271*, 11291−11300.
9. Reese-Wagoner, A., Thompson, J., and Banaszak, L. (1999) Structural properties of the adipocyte lipid binding protein, *Biochim. Biophys. Acta 1441*, 106−116.

10. Buelt, M. K., and Bernlohr, D. A. (1990) Modification of the adipocyte lipid binding protein by sulfhydryl reagents and analysis of the fatty acid binding domain, *Biochemistry 29*, 7408−7413.
11. Schoeffler, A. J., Ruiz, C. R., Joubert, A. M., Yang, X., and LiCata, V. J. (2003) Salt modulates the stability and lipid binding affinity of the adipocyte lipid-binding proteins, *J. Biol. Chem. 278*, 33268−33275.
12. Friedman, R., Nachliel, E., and Gutman, M. (2005) Protein surface: The dynamics of the interactions between protein, water and small solutes, *J. Biol. Phys.* (in press).
13. Zanotti, G., Feltre, L., and Spadon, P. (1994) A possible route for the release of fatty-acid from fatty-acid-binding protein, *Biochem. J. 301*, 459−463.
14. Arighi, C. N., Rossi, J. P. F. C., and Delfino, J. M. (1998) Temperature-induced conformational transition of intestinal fatty acid binding protein enhancing ligand binding: A functional, spectroscopic, and molecular modeling study, *Biochemistry 37*, 16802−16814.
15. Likic, V. A., and Prendergast, F. G. (1999) Structure and dynamics of the fatty acid binding cavity in apo rat intestinal fatty acid binding protein, *Protein Sci. 8*, 1649−1657.
16. Likic, V. A., Juranic, N., Macura, S., and Prendergast, F. G. (2000) A "structural" water molecule in the family of fatty acid binding proteins, *Protein Sci. 9*, 497−504.
17. Likic, V. A., and Prendergast, F. G. (2001) Dynamics of internal water in fatty acid binding protein: Computer simulations and comparison with experiments, *Proteins 43*, 65−72.
18. Bakowies, D., and van Gunsteren, W. F. (2002) Water in protein cavities: A procedure to identify internal water and exchange pathways and application to fatty acid-binding protein, *Proteins 47*, 534−545.
19. Bakowies, D., and van Gunsteren, W. F. (2002) Simulations of apo and holo-fatty acid binding protein: Structure and dynamics of protein, ligand and internal water, *J. Mol. Biol. 315*, 713−736.
20. Lindahl, E., Hess, B., and van der Spoel, D. (2001) Gromacs 3.0: A package for molecular simulation and trajectory analysis, *J. Mol. Mod. 7*, 306−317.
21. van Der Spoel, D., van Buuren, A. R., Apol, E., Meulenhoff, P. J., Tieleman, D. P., Sijbers, A. L. T. M., Hess, B., Feenstra, A. K., Lindahl, E., van Drunen, R., and Berendsen, H. J. C. (2002) *GROningen Machine for Chemical Simulations*, Department of Biophysical Chemistry, University of Groningen, Groningen, The Netherlands.
22. van Der Spoel, D., Lindahl, E., Hess, B., van Buuren, A. R., Apol, E., Meulenhoff, P. J., Tieleman, D. P., Sijbers, A. L. T. M., Feenstra, A. K., van Drunen, R., and Berendsen, H. J. C. (2004) *GROningen Machine for Chemical Simulations*, Department of Biophysical Chemistry, University of Groningen, Groningen, The Netherlands.
23. van Gunsteren, W. F., and Berendsen, H. J. C. (1987) *Gromos-87 Manual*, Biomos BV, Groningen, The Netherlands.
24. van Buuren, A. R., and Berendsen, H. J. C. (1993) Molecular dynamics simulation of the stability of a 22 residue α-helix in water and 30% trifluoroethanol, *Biopolymers 33*, 1159−1166.
25. van Buuren, A. R., Marrink, S. J., and Berendsen, H. J. C. (1993) A molecular dynamics study of the decane/water interface, *J. Phys. Chem. 97*, 9206−9212.
26. Mark, A. E., van Helden, S. P., Smith, P. E., Janssen, L. H. M., and van Gunsteren, W. F. (1994) Convergence properties of free energy calculations: α-Cyclodextrin complexes as a case study, *J. Am. Chem. Soc. 116*, 6293−6302.
27. Liu, H., Muller-Plathe, F., and van Gunsteren, W. F. (1995) A force field for liquid dimethyl sulfoxide and liquid proporties of liquid dimethyl sulfoxide calculated using molecular dynamics simulation, *J. Am. Chem. Soc. 117*, 4363−4366.
28. Berman, H. M., Westbrook, J., Feng, Z., Gilliland, G., Bhat, T. N., Weissig, H., Shindyalov, I. N., and Bourne, P. E. (2000) The Protein Data Bank, *Nucleic Acids Res. 28*, 235−242.
29. van Aalten, D. M. F., Bywater, R., Findlay, J. B. C., Hendlich, M., Hooft, R. W. W., and Vriend, G. (1996) PRODRG, a program for generating molecular topologies and unique molecular descriptors from coordinates of small molecules, *J. Comput.-Aided Mol. Des. 10*, 255−263.
30. Berendsen, H. J. C., Postma, J. P. M., van Gunsteren, W. F., and Hermans, J. (1969) Interaction Models for Water in Relation to Protein Hydration, *Nature 224*, 175−177.
31. Hess, B., Bekker, H., Berendsen, H. J. C., and Fraaije, J. G. E. M. (1997) LINCS: A linear constraint solver for molecular simulations, *J. Comput. Chem. 18*, 1463−1472.
32. Miyamoto, S., and Kollman, P. A. (1992) SETTLE: An Analytical Version of the SHAKE and RATTLE Algorithms for Rigid Water Models, *J. Comput. Chem. 13*, 952−962.
33. Berendsen, H. J. C., Postma, J. P. M., DiNola, A., and Haak, J. R. (1984) Molecular dynamics with coupling to an external bath *J. Chem. Phys. 81*, 3684−3690.
34. Darden, T., York, D., and Pedersen, L. (1993) Particle mesh Ewald: An n-log(n) method for Ewald sums in large systems, *J. Chem. Phys. 98*, 10089−10092.
35. Glaser, F., Pupko, T., Paz, I., Bell, R. E., Bechor-Shental, D., Martz, E., and Ben-Tal, N. (2003) ConSurf: Identification of functional regions in proteins by surface-mapping of phylogenetic information, *Bioinformatics 19*, 163−164.
36. Humphrey, W., Dalke, A., and Schulten, K. (1996) VMD: Visual molecular dynamics, *J. Mol. Graphics 14*, 33−38.
37. Cabani, S., Gianni, P., Mollica, V., and Lepori, L. (1981) Group contributions to the thermodynamic properties of nonionic organic solutes in dilute aqueous solution, *J. Solut. Chem. 10*, 563−595.
38. Mallard, W. G., and Linstrom, P. J., Eds. (1997) NIST Standard Reference Database, National Institute of Standards and Technology, Gaithersburg, MD.
39. Richieri, G. V., Ogata, R. T., and Kleinfeld, A. M. (1994) Equilibrium constants for the binding of fatty acids with fatty acid-binding proteins from adipocyte, intestine, heart, and liver measured with the fluorescent probe ADIFAB, *J. Biol. Chem. 269*, 23918−23930.
40. Richieri, G. V., Ogata, R. T., and Kleinfeld, A. M. (1995) Thermodynamics of fatty acid binding to fatty acid-binding proteins and fatty acid partition between water and membranes measured using the fluorescent probe ADIFAB, *J. Biol. Chem. 270*, 15076−15084.
41. Richieri, G. V., Low, P. J., Ogata, R. T., and Kleinfeld, A. M. (1998) Thermodynamics of fatty acid binding to engineered mutants of the adipocyte and intestinal fatty acid-binding proteins, *J. Biol. Chem. 273*, 7397−7405.
42. Ory, J. J., and Banaszak, L. J. (1999) Studies of the ligand binding reaction of adipocyte lipid binding protein using the fluorescent probe 1, 8-anilinonaphthalene-8-sulfonate, *Biophys. J. 77*, 1107−1116.
43. Becker, O. M., MacKerrel, A. D., Roux, B., and Watanabe, M., Eds. (2001) *Computational Biochemistry and Biophysics*, Marcel Dekker, New York.
44. Norberg, J., and Nilsson, L. (2003) Advances in biomolecular simulations: Methodology and recent applications, *Q. Rev. Biophys. 36*, 257−306.
45. Zimmerman, A. W., Rademacher, M., Ruterjans, H., Lucke, C., and Veerkamp, J. H. (1999) Functional and conformational characterization of new mutants of heart fatty acid-binding protein, *Biochem. J. 344*, 495−501.
46. Lucke, C., Rademacher, M., Zimmerman, A. W., van Moerkerk, H. T. B., Veerkamp, J. H., and Ruterjans, H. (2001) Spin-system heterogeneities indicate a selected-fit mechanism in fatty acid binding to heart-type fatty acid-binding protein (H-FABP), *Biochem. J. 354*, 259−266.
47. Hodsdon, M. E., and Cistola, D. P. (1997) Ligand binding alters the backbone mobility of intestinal fatty acid-binding protein as monitored by N-15 NMR relaxation and H-1 exchange, *Biochemistry 36*, 2278−2290.
48. Hodsdon, M. E., and Cistola, D. P. (1997) Discrete backbone disorder in the nuclear magnetic resonance structure of apo intestinal fatty acid-binding protein: Implications for the mechanism of ligand entry *Biochemistry 36*, 1450−1460.
49. Zimmerman, A. W., Rademacher, M., Ruterjans, H., Lucke, C., and Veerkamp, J. H. (1999) Functional and conformational characterization of new mutants of heart fatty acid-binding protein, *Biochem. J. 344* 495−501.
50. Sacchettini, J. C., Gordon, J. I., and Banaszak, L. J. (1989) Crystal-Structure of Rat Intestinal Fatty-Acid-Binding Protein: Refinement and Analysis of the *Escherichia coli*-Derived Protein with Bound Palmitate, *J. Mol. Biol. 208*, 327−339.
51. Richieri, G. V., Low, P. J., Ogata, R. T., and Kleinfeld, A. M. (1999) Fatty acid interactions with native and mutant fatty acid binding proteins, *Biochemistry 38*, 5888−5895.

BI048236T